



# Volatile Lubricants Injected Through Laser Drilled Micro Holes Enable Efficiently Hydrocarbon-Free Lubrication for Deep Drawing Processes

Paul Reichle<sup>1</sup> · Gerd Reichardt<sup>2</sup> · Manuel Henn<sup>3</sup> · Georg Umlauf<sup>4</sup> · Jakob Barz<sup>1,4</sup> · Kim Rouven Riedmüller<sup>2</sup> · Mathias Liewald<sup>2</sup> · Günter E. M. Tovar<sup>1,4</sup>

Received: 12 October 2022 / Revised: 3 January 2023 / Accepted: 6 February 2023 / Published online: 15 February 2023  
© The Author(s) 2023

## Abstract

In order to reduce the use of classic lubricants such as synthetic or mineral oils, emulsions or waxes in the deep drawing process, a new tribological system based on volatile lubricants was investigated. In this system, a volatile medium is injected under high pressure through laser drilled micro holes directly into the contact zone between the tool and the sheet metal and serves as a temporary lubricant. In order to investigate this tribological system under realistic conditions, strip drawing experiments with different volatile lubricants (air, nitrogen, carbon dioxide and argon) were performed on galvanized sheets. Therefore, a new generation of strip drawing tools was designed and numerically calculated for low elastic deformations to ensure a uniform contact pressure distribution over the entire friction contact area. To obtain a homogeneous distribution of the volatile lubricants, a number of micro holes with a depth of several millimeters were drilled into the hardened strip drawing jaws using ultrashort pulsed laser radiation. Taking into account the capabilities of this laser drilling technique in terms of size and shape of the micro holes, computational fluid dynamics simulations were performed to predict the flow behavior of the lubricant within the micro hole as well as the contact zone and were compared with observable effects in outflow tests. The chemical composition of the acting tribological layers was characterized by means of X-ray photoelectron spectroscopy and their changes during the deep drawing process were correlated with the lubricants used as well as the measured wear and friction values.

**Keywords** Dry forming · Volatile lubricants · Dry ice · Friction and wear · Gas lubrication · Strip drawing

## 1 Introduction

In metal forming processes, especially in deep drawing, it is necessary to use lubricants for reducing friction and wear in order to prevent damage of the tools and the formed sheet metal. The lubricants used for this purpose are typically

hydrocarbon based oils (synthetic or mineral), waxes or emulsions. Frequently, other substances with harmful impacts on the environment and human health are added [1]. In any case, it is necessary to apply the lubricant to the sheet metal prior to the forming process and remove it subsequently to enable further process steps like coating or bonding. To avoid the need of these lubricants and to reduce the process effort, science is investigating in new dry metal forming techniques [2]. The usual approaches for solving this problem are coatings and surface structures. Böhmermann et al. [3] designed structured and diamond-like carbon hard coated dies for dry rotary swaging. Especially when forming aluminum or zinc-coated sheet metal, adhesive wear is a difficulty. Zhao et al. [4] investigated the influence of an amorphous hydrogenated carbon coating on the tribological conditions by deep drawing of aluminum. These two investigations are exemplary for the realization of a dry forming process without any use of lubricants. In contrast, Vollertsen et al. [1] defines a dry metal forming technology as a

✉ Paul Reichle  
paul.reichle@igvp.uni-stuttgart.de

<sup>1</sup> Institute of Interfacial Process Engineering and Plasma Technology (IGVP), University of Stuttgart, Nobelstrasse 12, 70569 Stuttgart, Germany

<sup>2</sup> Institute for Metal Forming Technology (IFU), University of Stuttgart, Holzgartenstrasse 17, 70174 Stuttgart, Germany

<sup>3</sup> Institut für Strahlwerkzeuge (IFSW), University of Stuttgart, Pfaffenwaldring 43, 70569 Stuttgart, Germany

<sup>4</sup> Fraunhofer Institute for Interfacial Engineering and Biotechnology (IGB), Nobelstrasse 12, 70569 Stuttgart, Germany

process with no need of further process steps like cleaning or drying prior to painting, joining, etc., which means that it is not necessary to forgo lubricants at all. In the approach presented here, volatile substances are used to lubricate the sheet metal forming process. Therefore, the medium is introduced to the contact zone via laser drilled micro holes inside the tool (cf. Fig. 1 and Sect. 2.2) and operates as a temporary lubricant. Previous investigations working with nitrogen ( $N_2$ ) and carbon dioxide ( $CO_2$ ) showed highly promising results regarding wear, friction and consequently an enlarged process window in deep drawing [5, 6]. When using volatile lubricants during the deep drawing procedure, the process chain can be reduced, eliminating now redundant steps like oil application, component cleaning and the expensive disposal of cleaning residues. Furthermore, the avoidance of lubricant additives that are harmful to human health, such as chlorinated paraffins, can be mentioned. From the ecological point of view, these can lead to positive effects compared to commercial lubricants. Peng et al. [7] and Pereira et al. [8] investigated the impact of liquid  $CO_2$  and  $N_2$  for cleaning and lubricating purposes on the environment. To evaluate the environmental impact of  $CO_2$  as volatile lubricant, it is indispensable to take a look at the extraction method of the used  $CO_2$ . Ideally, used  $CO_2$  is taken as a waste product from other processes, such as bioethanol plants, ammonia synthesis or technical combustion processes for use as a volatile lubricant. This way, the additional emission of greenhouse gases can be reduced. However, further efforts must be made to recycle, to reduce the usage or to use other volatile lubricants such as compressed air or  $N_2$  to generate a lower impact on the environment. Therefore, this research was made to investigate the lubrication effects of different volatile lubricants.

Since Bowden [10] and Mishina [11] researched in the field of friction and wear of dry metal sliding contacts under different environments, several investigations followed [12–16] and showed a dependency on the surrounding atmosphere for the tribological conditions. Besides the therein presented effects, the fluid flow properties of

different volatile lubricants have been investigated in this research, as they play a key part of effects on tribology. Therefore, computational fluid dynamics simulations (CFD) of the lubricants flow behavior were carried out (Sect. 3.1). To investigate the interactions of the different effects, strip drawing tests with tailor-made drawing jaws (Sect. 2.1) were performed with dry (technical) air, liquid  $CO_2$ ,  $N_2$  and argon (Ar) as volatile lubricants to examine friction and wear for deep drawing purposes. The friction was measured by force sensors during the process and wear was classified by roughness and gloss measurements (Sect. 3.2). To investigate chemical changes of the surfaces as a result of drawing and lubrication process, X-ray photoelectron spectroscopy (XPS) measurements were performed (Sect. 3.3).

## 2 Materials and Methods

### 2.1 Design of Strip Drawing Jaws

For the tribological investigations, a conventional strip drawing device was modified in order to analyse the influences of different volatile lubricants on the coefficient of friction, on tribological failures and on tribo-chemical reactions. The modification includes the integration of a media supply via an adapter on the drawing jaw and the elasto-mechanic dimensioning of the drawing jaws themselves. All drawing jaws were manufactured using the high-alloy cold-work tool steel 1.2379. This material is a common tool material used for the active components of metal forming tools. For a long durability of the drawing jaws, they were fully hardened to  $60 \pm 2\text{HRC}$  in a vacuum hardening process. The resulting slight thermal distortion was compensated by grinding over the drawing jaws after the hardening process. The micro holes were laser drilled (cf. Sect. 2.2) after the drawing jaws had been hardened and ground in order to prevent the conical bore geometry from being negatively affected by a material loss due to the grinding process. Finally, the surfaces of the drawing jaws were polished to ensure a high surface

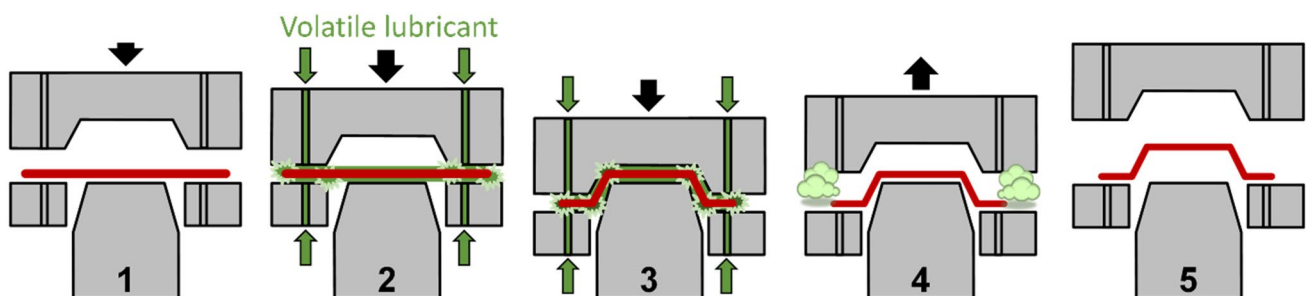


**Fig. 1** Schematic representation of the process steps (1–5) during deep drawing lubricated by volatile media injected through laser drilled micro holes (with permission [9])

quality. The new designed drawing jaws contain a media distribution and the integrated laser drilled micro holes on the contact surfaces (cf. Fig. 2). The position and the size of the friction surface on the drawing jaws as well as the number and positioning of the micro holes were taken from previous investigations in order to ensure comparability with past test results [6, 17–20]. The two contact surfaces of each drawing jaw were 10 mm wide and 20 mm long, respectively. The circumferential edges of the contact surfaces were rounded with a radius of 1 mm in order to avoid edge effects during the friction experiments. All drawing jaws thus provided a contact area of 400 mm<sup>2</sup>. Each contact surface of the

drawing jaw contained 3×3 micro holes, designed as a diffuser having an exit diameter of approx. 600 μm (cf. Fig. 4).

In the mechanical design of the drawing jaws, the geometry of themselves was optimized. The aim of the optimization was to reduce the elastic deformation of the drawing jaw, especially in the area of the friction surfaces. For this purpose, the elastic deformation was numerically calculated using ANSYS workbench, taking into account the fluid pressure and the contact pressure as loads. Due to the maximum possible laser drilling depth of 5 mm for the micro holes specified at the time of development, the material thickness in the area of the

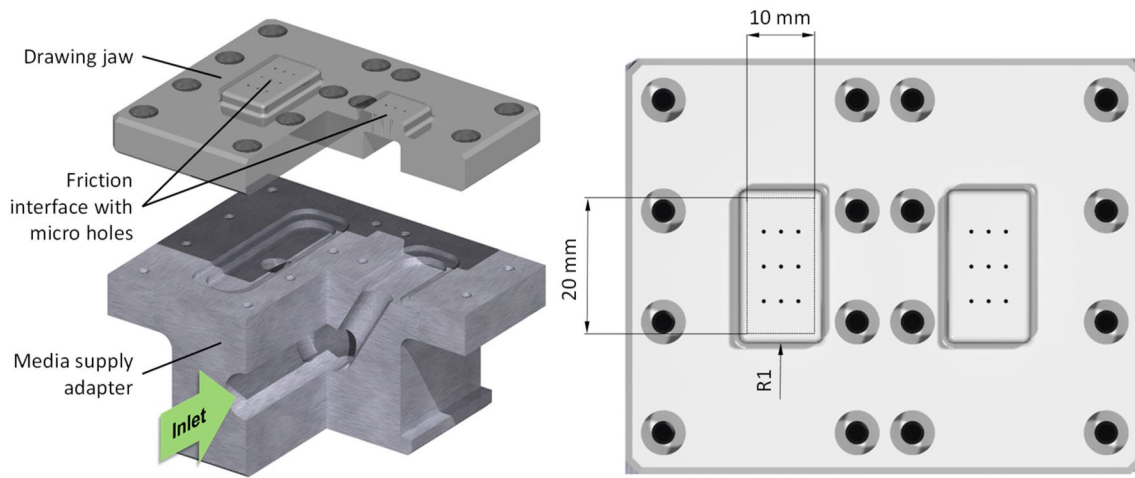


**Fig. 2** Drawing jaw and adapter with media supply of the strip drawing investigations

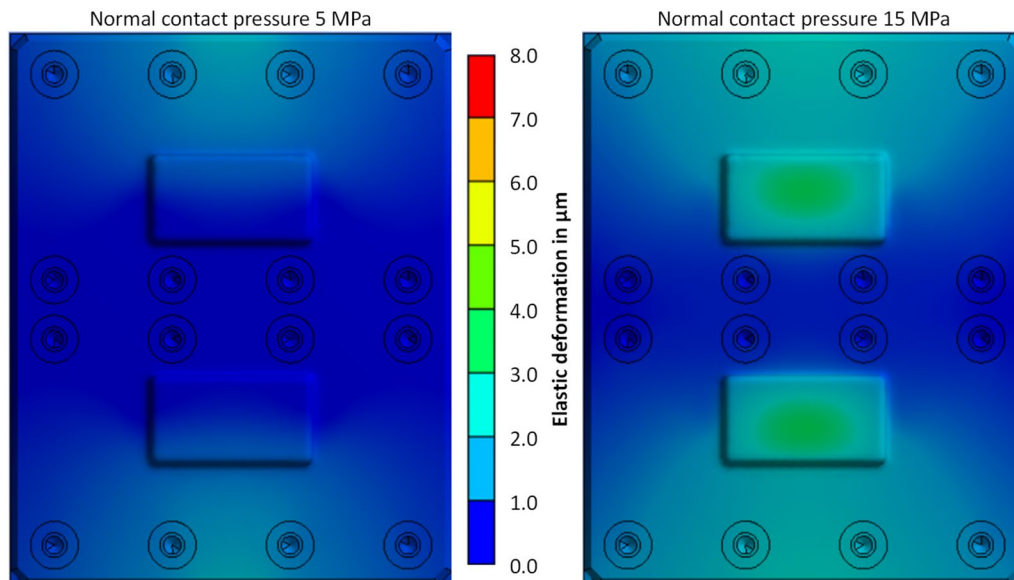


**Fig. 3** Simulation of the elastic deformation in micrometers of the 5 mm thick drawing jaw at a contact pressure of 5 and 15 MPa and an internal fluid pressure of 10 MPa (full colored figure online)

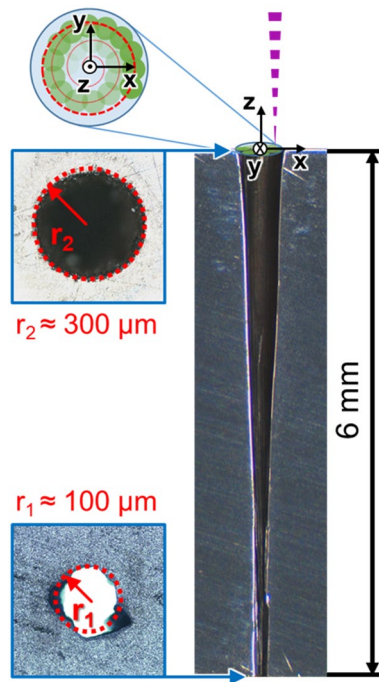


**Fig. 4** Cross section of a micro hole (right) in hardened cold-work steel (1.2379), produced with the setup and drilling strategy described in detail in Reichardt et al. [6]. The dotted circles in the images of the opening of the gas inlet (bottom left) and the gas outlet (top left) represent equivalent cross sectional areas where the radius equals approx.  $r_1 = 100 \mu\text{m}$  and  $r_2 = 300 \mu\text{m}$ , respectively

contact surface was not allowed to exceed this value for the optimization. Improvements of the laser technology allowed deeper micro holes up to a depth of 6.7 mm later on in the investigations. The final geometry of the drawing jaw including the adapter for the gas supply can be seen in Fig. 2.

The elastic deformation of the drawing jaw was numerically calculated with the high fluid pressure of 10 MPa (100 bar), also considering the bolted media supply adapter. In the simulation, a contact pressure of 5 MPa (left in Fig. 3) and 15 MPa (right in Fig. 3) was considered on the contact zones. At a contact pressure of 5 MPa, the maximum elastic deformation in the area of the contact surfaces was calculated very low at  $1.3 \mu\text{m}$ . Even at the higher contact pressure of 15 MPa (Fig. 3 right), the maximum elastic deformation of  $2.35 \mu\text{m}$  was in a very low range, so that a negative influence of an irregularly located contact pressure distribution on the contact zone could be excluded. Consequently, valid investigations for the friction characterisation of considered volatile tribological systems in sheet metal forming could be carried out using the developed drawing jaw design.

## 2.2 Laser Drilling of the Micro Holes

The production of longitudinally shaped micro holes with high aspect ratios holds many challenges. Conventional ultrashort pulse lasers typically are not suited to drill deep micro holes, since they only generate pulses with an energy in the range of a few hundred microjoules. Only recently, lasers capable of generating pulses with higher energy in the range of millijoules are slowly coming onto the market. However, the use of high pulse energy in combination with high pulse repetition rates can lead to damage of the hardened tool steel due to heat accumulation [21].

Several analytical models were developed to assist in the design of the drilling process and to meet the requirements for the geometry of the diffuser-shaped micro holes. The ablation diameter, i.e. entrance of the micro hole on the side of the laser impact can be calculated analytically [19]. The aspect ratio between the ablation diameter and the drilling depth are interdependent and result in a conical micro hole shape. For percussion drilling, the quality depth limit can be analytically predicted [22]. Based on this prediction an analytical model for the depth progress of percussion drilled micro holes was developed [23].

A depth-adapted drilling strategy was used in which the focus of the laser beam was moved along a spiral path and the focal plane was incrementally shifted below the surface of the strip drawing jaws [6]. For this purpose, a kW-class ps-laser (construction of the IFSW [24]) was used in combination with a galvanometer scanner and a telecentric f-theta lens. The laser produced pulses with a pulse duration of 8 ps and a pulse energy of approx. 2.8 mJ. In order to avoid heat accumulation, the repetition rate was lowered to 30 kHz, resulting in an average laser power of about 84 W. An exemplary cross section of a drilled micro hole using the aforementioned strategy is depicted in Fig. 4.

## 2.3 Experimental Setup of Strip Drawing Investigations and Sample Preparation

All experimental investigations followed the same procedure. The mechanically and chemically cleaned sheet samples (electrolytic galvanized cold rolled steel sheets DC05+ZE, residual oil quantity lower than  $0.1 \text{ g m}^{-2}$ ,  $50 \text{ mm} \times 500 \text{ mm}$ ) were mounted on the slide of the strip drawing testing rig. Then the drawing jaw was lowered onto the sheet metal specimen with the set contact pressure ( $p_N = 5$  or  $15 \text{ MPa}$ ) and the media feed was activated. At a constant drawing speed of 100 mm per second, the normal and friction forces were measured using piezo-electric force washers in order to calculate the friction coefficient  $\mu$  using the friction model of Coulomb. To assess the wear of the drawn sheets, surface roughness measurements (on an area of  $15.5 \text{ mm}^2$ ) were performed using a 3D-confocal

microscope (nanofocus usurf mobile). The measuring accuracy can be estimated on the basis of the measuring uncertainty (calibrated according to German standard VDE/VDI 2655-1.2) and the repeatability to a deviation of  $\pm 0.04 \mu\text{m}$ . As the aged zinc oxide and zinc carbonate surfaces are dull and the bare zinc is shinier, gloss measurements of the worn strips after the standard DIN EN ISO 2813:2015-02 were performed, besides the roughness measurements, to evaluate wear. For this purpose, the RHOPOINT IQ goniophotometer was used, measuring the gloss of the sheet metal strips at an angle of  $60^\circ$  to the surface. The results are presented in gloss units (GU) and are calibrated to a highly polished black glass standard with 100 GU.

In the tribological investigations,  $\text{CO}_2$  (liquid),  $\text{N}_2$  (gaseous), Ar (gaseous) and compressed technical air (gaseous) were used as volatile lubricants. The gaseous fluids were tested for their suitability as volatile lubricants at a fluid pressure ( $p_F$ ) of 6 MPa (60 bar) and 10 MPa (100 bar). All fluids were taken from commercially available pressurised gas cylinders (purity  $\geq 99.7 \text{ vol}\%$ ) and fed to the drawing jaw via the adapter using an electromagnetic valve. For the gaseous fluids, the desired pressure of 6 MPa or 10 MPa was set on the pressurised gas cylinder by means of a pressure reducer. The  $\text{CO}_2$  was taken in liquid phase from the gas cylinder with a riser pipe. According to the  $p$ - $T$ -behaviour, the pressure of liquid  $\text{CO}_2$  at room temperature is approx. 6 MPa and cannot be changed. Thus, no investigations could be carried out with  $\text{CO}_2$  at a fluid pressure of 10 MPa. All 14 parameter combinations, as shown in Table 1, were repeated at least three times to ensure a statistical validation.

### 2.4 Simulation Model and Testing Method of Fluid Flow

To investigate the flow behavior of the lubricants in the micro hole and the contact zone between sheet metal and tool, computational fluid dynamics simulations were carried out. Previous studies examined the influence of the micro hole design on flow regime and lubrication effects and identified a constantly widening diameter in flow direction (here consistently called diffuser, like in subsonic flow velocities) as advantageous (cf. Figs. 4 and 5) [6, 25]. In contrast, the simulations of this investigation focus more on understanding the flow behavior of  $\text{CO}_2$  in the contact zone. For a validation of the results and to get a closer insight into the flow regime and phase changes of

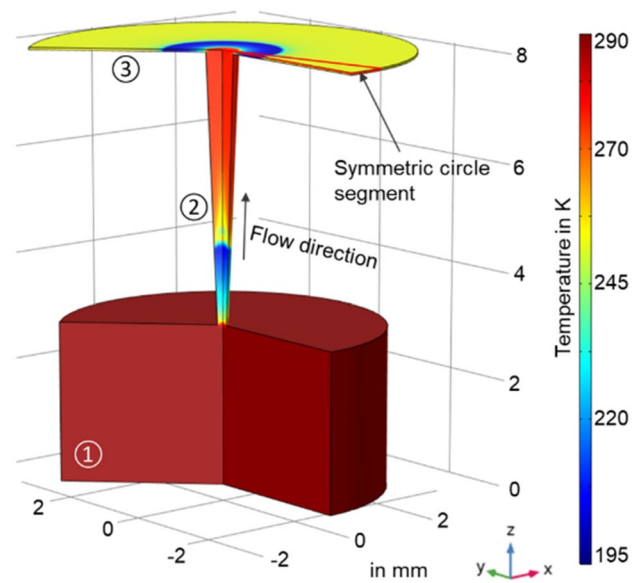


**Fig. 5** Three-dimensional computational fluid dynamics simulation of the  $\text{CO}_2$  flow inside feed ①, within the micro hole ② and in the contact zone ③. For a better clarity, the simulation shown here was performed without heat transfer to the surrounding material (full colored figure online)

$\text{CO}_2$ , outflow tests with a glass plate as a replacement for the sheet metal (further description see below and [25]) as well as temperature measurements in the contact zone were performed.

The CFD simulations were carried out using the finite element software COMSOL-Multiphysics and the open source program OpenFOAM. Since the volatile media accelerates inside the micro hole drastically, previous investigations showed a turbulent flow behavior. Thus, different flow equations for turbulent fluids had been compared and the preliminary tests showed a sufficient accuracy for the  $k$ - $\epsilon$  turbulence model compared to the moderate computing effort [6]. For validation, single results were also simulated using the Large-Eddy turbulence model, which mostly confirmed the results of the  $k$ - $\epsilon$  turbulence model (for underlying equations see [26]). Because of the proximity to the critical point of the used  $\text{CO}_2$ , its compressibility factor was included into the model. Thus, to calculate the fluid pressure  $p$ , the Peng-Robinson equation, which describes gaseous and liquid state, was implemented as follows [27]:

**Table 1** Investigated parameter combinations of strip drawing experiments ( $n \geq 3$ )

Experiment number	1	2	3	4	5	6	7	8	9	10	11	12	13	14
Volatile lubricant—fluid	$\text{CO}_2$	$\text{CO}_2$	$\text{N}_2$	$\text{N}_2$	$\text{N}_2$	$\text{N}_2$	Ar	Ar	Ar	Ar	Air	Air	Air	Air
Fluid pressure in MPa	6	6	6	6	10	10	6	6	10	10	6	6	10	10
Contact pressure in MPa	5	15	5	15	5	15	5	15	5	15	5	15	5	15

$$p = \frac{R \cdot T}{V_m - b} - \frac{a \cdot \alpha}{V_m^2 + 2b \cdot V_m + b^2} \quad (1)$$

in combination with the equations of the intermolecular attraction parameter  $a$  and the excluded co-volume  $b$ :

$$a = \frac{0.45724 \cdot R^2 \cdot T_c^2}{p_c} \quad (2)$$

$$b = \frac{0.0778 \cdot R \cdot T_c}{p_c} \quad (3)$$

whereby  $R$  is the molar gas constant,  $T$  the fluid temperature,  $V_m$  the molar volume,  $\alpha(T_r, \omega)$  a dimensionless function of the reduced temperature and the acentric factor (here  $\alpha \approx 1.23$ ),  $T_c$  and  $p_c$  the temperature and pressure of the critical point, respectively. As the  $\text{CO}_2$  was extracted in its liquid state from the gas cylinder at approx. 6 MPa, the inlet pressure of all lubricants was set to this value. Ambient conditions were defined as outlet pressure. The viscosity of the lubricants was calculated by the Sutherland's law in dependency of the lubricant's temperature. The starting temperature of the lubricant, tool and sheet metal was set to room temperature. Different measurements by infrared thermography, thermocouple and pyrometer showed only a low decrease of the tool temperature during the process, thus the tool temperature was set constant in the simulations. Instead of the surface roughness, a no slip condition was implemented.

$\text{CO}_2$  changes its physical state during the lubrication process. In the feed, it is in the liquid state and changes during the process partially and temporarily to its solid state before evaporating completely. Except for  $\text{CO}_2$ , no lubrication fluid of this research has a phase change in the processing area. Thus, the flow behavior of these media differs only because of different heat capacities, viscosities and compressibility factors. In contrast, the simulation of  $\text{CO}_2$ , including phase changes and multiphase flow, is much more challenging. Several approaches like using the Peng-Robinson equation of state (1)–(3) were implemented; however, as outlined a series of simplifications must be made. Thus, the shown CFD results (cf. Sect. 3.1) are focusing on the usage of  $\text{CO}_2$ , which can be validated by visible effects in outflow experiments. Due to the replacement of the sheet metal by a glass plate in the lubrication process, the solid phase can be examined at the micro hole's outlet. Therefore, a jaw with only one laser drilled micro hole was connected to the lubricant feed. The variation of the contact pressure between glass plate and tool is realized in this case by four screws. To observe the flow behavior of the  $\text{CO}_2$ , a high-speed camera (Photonfocus MV1) was installed below the assemblage.

## 2.5 Chemical Surface Analysis—Examination Method and Background

The corrosion protective ability of zinc-coated surfaces is caused by an interaction of covering and sacrifice effect towards other metals. The dry top layer usually consists of zinc oxide ( $\text{ZnO}$ ) and zinc carbides ( $\text{ZnCO}_3$ ) [28, 29]. To investigate any chemical changes on the surface of the sheets, initiated by the lubricated drawing procedure, Xray photoelectron spectroscopy (XPS) measurements were carried out. Therefore, the Kratos Axis Supra with implemented argon cluster gun and a maximum spot size of  $0.8 \text{ mm} \times 0.5 \text{ mm}$  was used. Because of the measuring method of detecting the emitted photoelectrons and Auger electrons following the irradiation with monochromatic X-rays, XPS yields chemical information on the upper 10–15 nm of the surface. During measurement, the samples must be held in an ultra-high vacuum at  $10^{-4} \text{ Pa}$ . For these investigations, approx.  $5 \text{ mm} \times 5 \text{ mm}$  pieces of the sheet samples, which were run over by the drawing jaw, were cut off. The measurements were made for all lubrication media on the samples drawn with the highest used contact and fluid pressure. This has been done, as chemical changes are more likely to occur on the surface of these sheet metal specimens. The samples are depicted and measuring spots are marked in Fig. 9. To reduce deposits from atmosphere on the freshly drawn strips, the samples were directly prepared after the drawing test and packed airtight until inserted into vacuum. For a better comparability, an aged, cleaned and not drawn sheet specimen also was measured as a reference.

## 3 Results and Discussion

### 3.1 Simulation and Outflow Tests of the Fluid Behavior in Micro Hole and Contact Zone

The investigation of the lubricant flow in tool and contact zone was carried out for all media used in this work. As mentioned before, here the main focus was put on the usage of  $\text{CO}_2$  as it is the most challenging calculation and the results can be compared to outflow tests (cf. Fig. 7). In Fig. 5 a 3D-simulation model of the  $\text{CO}_2$  lubricant in the supply channel ①, micro hole ② and contact zone (gap between sheet metal and tool) ③ is shown. At the passage from supply channel to micro hole, the media passes the narrowest position and accelerates up to supersonic velocities. Thus, the pressure drops, leading in case of  $\text{CO}_2$  to evaporation processes. These processes, together with the Joule–Thomson effect, cause a drastical temperature drop to around 200 K of the medium. The cooling can surmount the released energy of crystallization, leading to small dry ice flakes. Dependent on the flow properties in the contact zone,

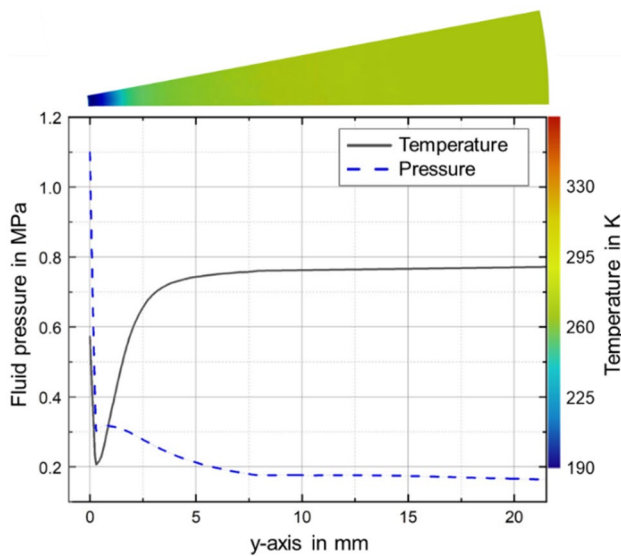


**Fig. 6** Simulation result of CO<sub>2</sub> pressure and temperature curve originating from the center and outlet of the micro hole in the contact zone. For a better clarity, a symmetric circle segment of the simulation is shown at the top (full colored figure online)

a compression shock wave arises in the micro hole, which triggers a sudden increase of pressure and temperature.

The applied contact pressure, the roughness of the contact bodies, the used sheet material and the supply pressure of the lubricant mainly influence the height of the contact zone (distance between tool and sheet metal surface). The height itself has a major impact on the lubricant flow, which in turn influences the tribology conditions. In Fig. 6 the pressure and temperature curve along the radius, originating from the micro hole's center, for CO<sub>2</sub> and a 10 μm high contact zone is outlined. A symmetric circle segment is shown at the top to illustrate the position in the 3D-CFD model. At the passage from micro hole to the contact zone, the lubricant accelerates again and similar effects like at the supply side of the micro hole occur. However, the fluid pressure drops below the limit when liquid CO<sub>2</sub> can be present, wherefore all lubricant exists now in solid or gaseous state. If the contact zone is of marginal height, the compression shock wave can move from the micro hole to the contact zone. In addition, heat exchange effects between fluid, tool and sheet metal lead to a rise of temperature of the lubricant, effecting evaporation processes and thus a delayed pressure decrease. In general, as described, the tool and sheet temperature are not decreasing significantly, although single roughness peaks (asperities) exposed to the cold lubricant flow can cool down to temperatures below 220 K, due to the high medium velocity and fast heat transfer effects. For validation of this numerical result, thermocouple experiments inside the contact zone were performed showing minimum material temperatures of around 233 K. However, as the temperature

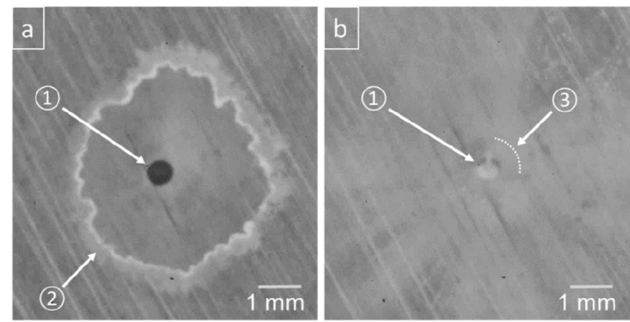


**Fig. 7** Top view of the micro hole ① to investigate the CO<sub>2</sub> flow and the point with the highest amount of dry ice formation ② and ③ (circle segment to guide the eye) inside the contact zone: **a** regime with no continuous flow; **b** approximately steady flow conditions during drawing process

was measured in a distance of around 2 mm from the micro hole and the thermocouple was covered by a 0.1 mm thick copper foil, significant lower temperatures are expected directly at the interfaces in the contact zone.

In contrast to the lubrication with liquid CO<sub>2</sub>, the temperature stays above 270 K (cooling of Joule–Thomson effect) when using one of the other described gaseous media. Furthermore, the simulations showed a higher pressure inside the contact zone when using CO<sub>2</sub> (micro hole outlet pressure approx. 4.1 MPa) in comparison to the other media. This can be explained based on a higher mass flux of liquid CO<sub>2</sub> at the entrance of the micro hole. The micro hole outlet pressure of the other investigated media is almost similar as the results for air, N<sub>2</sub> (both approx. 3.3 MPa) and Ar (3.1 MPa) show. The lower pressure for Ar is caused by a slightly lower gas temperature as a result of the Joule–Thomson effect. As the motion of the sheet metal is neglected in the simulations, the load carrying capacity (acting force, pushing the counter bodies apart) for one micro hole is independent of the viscosity of the fluid. Hence, the fluid pressure in the contact zone has the major impact on the load carrying capacity, comparable to an external pressurized hydrostatic bearing [30]. In Wörz et al. [31] pressure tests in the contact zone were performed, showing comparable results regarding the relation between used lubricants and load carrying capacity, validating the here shown simulative results.

The outflow tests, illustrated in Fig. 7, show mainly two different flow regimes: (a) An unstable operating point where the process pressure or the height of the contact zone is low, resulting in an unsteady and low dry ice formation limited to the contact zone. In (b) an almost stable operation point is shown, which is found during the usual drawing process (fluid pressure 6 MPa, contact pressure 5 MPa). The whitish color of the center shows a high dry ice formation within the micro hole. Hence, the temperatures at this point have to be lower than 218 K. Although the simulation showed slightly higher

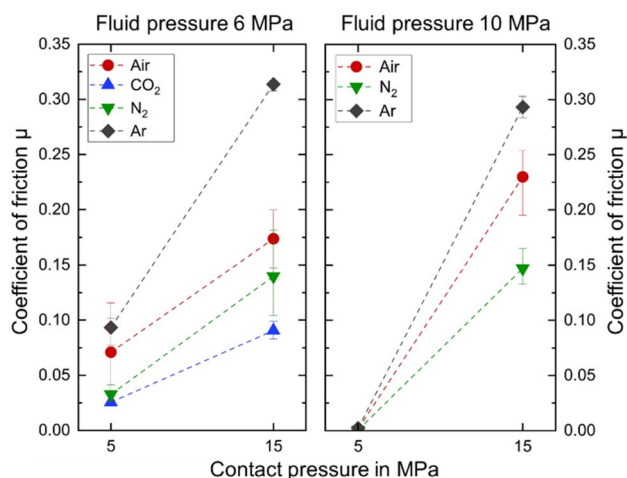


**Fig. 8** Coefficient of friction for different contact and fluid pressures. Left: Fluid pressure 6 MPa. Right: Fluid pressure 10 MPa (error bars min. and max. values; dashed lines only to guide the eye)

temperatures, which can be explained by the implemented constant tool temperature, this study validates the previously shown simulation results. Based on these  $p$ - $T$ -results of the simulation, the highest amount of dry ice was assumed around 0.5 mm after the exit of the micro hole. This can also be seen as a faint circle around the micro hole in the outflow tests at point 3 in Fig. 7b. After this position, the simulation showed a rapidly ongoing warming (heat exchange with tool and sheet metal) and consequently sublimation processes. In this extend, these effects could not be identified in the outflow tests, which can be also explained by decreasing surface temperatures in the experiments and simplifications, which were carried out in the simulation. Thus, the dry ice sublimates later (higher amount) inside the contact zone than expected from the simulation and is longer present to lubricate drawing processes. Inside the contact zone, single flow channels arise, following the lowest resistance through the surface roughness. The higher the applied contact pressure the narrower is the contact zone and the later  $\text{CO}_2$  changes its state from liquid to gaseous and solid, which can be seen in a lower amount of white color at the exit of the micro hole.

## 3.2 Strip Drawing Tests with Different Volatile Media

### 3.2.1 Friction During Drawing

The coefficients of friction determined during the strip drawing experiments using the volatile lubricants  $\text{CO}_2$  (liquid),  $\text{N}_2$ , Ar and compressed technical air at contact pressure values of 5 and 15 MPa are shown in Fig. 8. The sheet metal material DC05 + ZE and the tool material 1.2379 ( $60 \pm 2\text{HRC}$ ) were used for all investigations. The variation of the

results measured in this process is shown by the minimum and maximum deviation from the arithmetic mean as error bars in the diagrams of Fig. 8. The left diagram shows the results at a fluid pressure of 6 MPa and the right diagram shows the results at a fluid pressure of 10 MPa. Variance analysis (ANOVA) for this data showed no significant differences for the investigations at  $p_N = 5$  MPa. However, significant, e.g. highly significant, differences at  $p_N = 15$  MPa (except air- $\text{N}_2$  at  $p_F = 6$  MPa;  $p$ -values  $\leq 0.0004$ ) were measured.

To combine gained results, an increase in the coefficients of friction could be observed with increasing contact pressure for both fluid pressures investigated (6 and 10 MPa). In other studies, with higher contact pressures using a stretch bending testing rig adapted for volatile lubricants, it could be shown that the increase of the coefficients of friction did not continue continuously when increasing contact pressure in case of applying both  $\text{CO}_2$  and  $\text{N}_2$ . Thus, at higher contact pressures, a decrease of the coefficients of friction could be observed due to a sealing effect between the sheet and the tool surface, which improved the lubrication effect in the contact zone [32]. The coefficients of friction were remarkably low for all gaseous lubricants at a fluid pressure of 10 MPa and a contact pressure of 5 MPa. Here, the friction coefficients were almost zero, which means that there was effectively no friction between both contact partners. The reason for this effect was found in the mechanical stress equilibrium between the load carrying capacity (separating effect of the fluid pressure) and the contact stress applied by the strip drawing device. The fluid pressure in this experimental series was set on the fluid inlet side to 10 MPa and was therefore twice as high as the contact pressure of 5 MPa. This caused the friction partners to separate from each other (lift off), whereby the lifting height adjusted itself in such a way that the average fluid pressure in the contact zone corresponded exactly to the set contact pressure of the strip drawing rig (cf. Sect. 3.2.2 and [9]).

For both fluid pressures of 6 and 10 MPa, the same order of the results for the investigated lubricants with regard to the level of the coefficient of friction could be observed.  $\text{CO}_2$  ( $p_F = 6$  MPa) reduced the friction most effectively down to  $\mu = 0.026$  at a contact pressure of 5 MPa. At a contact pressure of 15 MPa,  $\text{CO}_2$  provided a coefficient of friction with a value of 0.09 at a low level.

$\text{N}_2$  was found as the second most suitable fluid for friction reduction. The coefficient of friction here ranged between  $\mu = 0.032$  and  $\mu = 0.147$ . Increasing the fluid pressure of  $\text{N}_2$  did not reduce the absolute coefficient of friction. However, the scatter of the repeat measurements (cf. error bar in Fig. 8) decreased significantly and thus the stability of the friction process increased with increasing fluid pressure. Though, slight adhesions on the contact surfaces of the drawing jaw occurred when applying both levels of



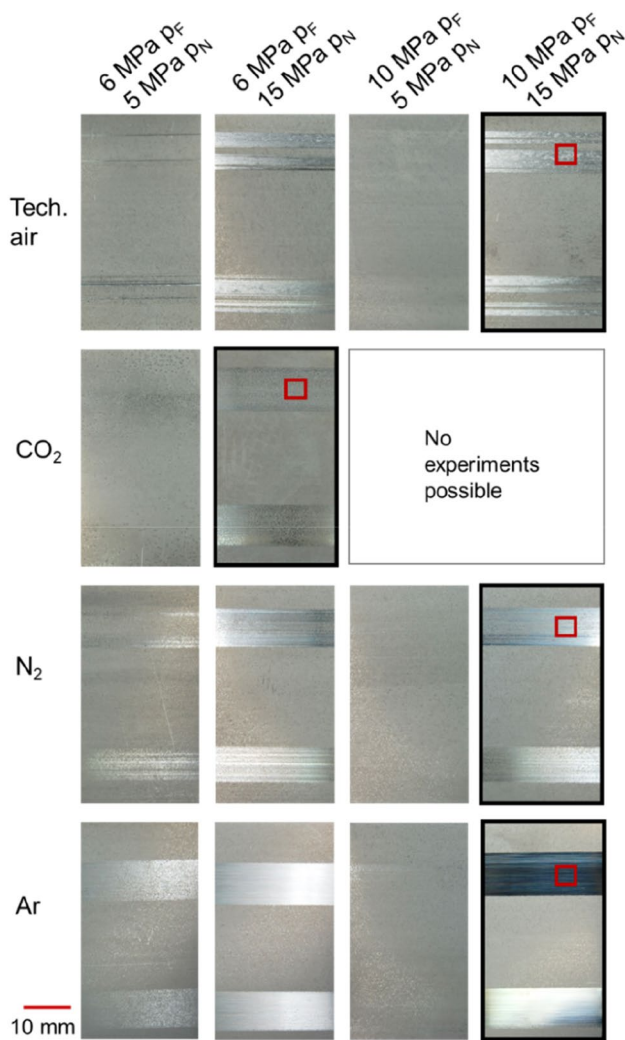


**Fig. 9** Images of the worn sheet metal surfaces from strip drawing tests under different lubrication media, fluid pressures ( $p_F$ ) and contact pressures ( $p_N$ ). The framed samples were chemically examined via XPS in the marked squares

fluid pressure, in each case at the higher contact pressure of 15 MPa. Thus, a process-safe use of this fluid under current circumstances is to be evaluated as critical and is only an option for low contact pressures.

Both technical compressed air ( $\mu_{max} = 0.230$ ) and pure Ar ( $\mu_{max} = 0.314$ ) showed very high coefficients of friction. With compressed air, however, slight to strong adhesion formation on the strip drawing jaw occurred. The oxygen content in the technical compressed air has a strong negative influence on the friction process (cf. Sects. 3.2.2 and 3.3). This thesis is proven by the direct comparison of the coefficient of friction of compressed air with pure  $N_2$  depicted in Fig. 8. The used technical compressed air consists of 79%  $N_2$  and 21%  $O_2$  and differs from pure  $N_2$  only in the  $O_2$  content. It does not contain any inert gases or  $CO_2$  in significant amounts. The friction coefficients of compressed air for all

parameter combinations were measured far above those of  $N_2$ , as depicted in Fig. 8. In addition, the flow properties (heat capacity, viscosity and compressibility factor) of the contained oxygen cause no remarkable differences in flow behavior compared to  $N_2$ . This means that the strong adhesion and abrasion formation and the higher coefficient of friction can clearly be attributed to the negative influence of oxygen in technical compressed air.

Another finding of these investigations was that only low adhesion phenomena occurred on the drawing tools with Ar, despite the highest friction coefficients. This can also be recognized in the diagrams in Fig. 8 from the small error bars. Thus, Ar as volatile lubricant caused high coefficients of friction, but with relatively stable process behavior.

### 3.2.2 Evaluation of Wear Formation

Besides the friction coefficients, the evaluation of wear as a result of the drawing process is an important factor to assess emerging lubrication effects of the different volatile media. In Fig. 9, images of the worn zinc-coated strips under different lubrication conditions and contact pressures are shown. The framed samples and areas indicate the measuring spots for the subsequently described XPS investigations. In the images it can be seen, that an increase of contact pressure led to heavier wear in case of all trials. In accordance with the friction coefficients, a lift off of the tool as a result of high fluid pressure and low contact pressure prevent solid contact between both counter bodies and thus any direct wear. The results correlate with the CFD simulations and calculations for a lift off made in Liewald et al. [9]. For 6 MPa fluid pressure the tool starts to lift partially from 5.1 MPa normal pressure on. As discussed, the limit was found approx. 15% lower when using  $CO_2$  as lubricant because of a higher pressure (higher load carrying capacity) in the contact zone. For 10 MPa fluid pressure, this limit is around 7.5 MPa [9]. The measured averaged surface roughness  $S_a$  of the worn area, shown in Fig. 10, illustrates this relation. For all lubricants, except air,  $S_a$  decreased as the roughness peaks of the zinc-coated sheets were flattened. The increase of the surface roughness, when using air as lubricant, can be explained by high abrasive wear (creation of single deep wear scratches). Although, the deviation between the reference and the under air drawn specimens is on the lowest level (at  $p_F$  of 6 MPa) compared to the other lubricants, the calculation of the  $S_a$  value conceals the real depth of single scratches. As some parts of the surface were flattened and other parts roughened, the gloss measurements, illustrated in Fig. 11, show only a low increase of the gloss for air, too. As these separate deep scratches only occurred when using air, this effect is probable caused by the formation of ZnO from bare zinc and oxygen. Zinc oxide can be used for lubrication at elevated temperatures because of its thermal stability. However, at room

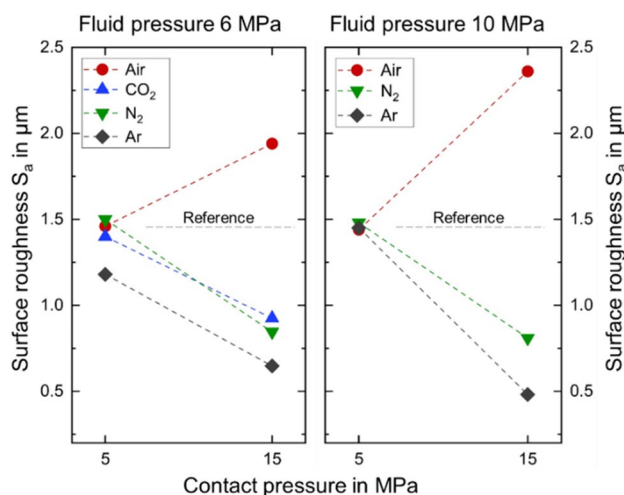


**Fig. 10** Averaged area roughness value of the sheet metal strips before (reference) and after drawing with various volatile lubricants at different contact—and fluid pressures (measuring area 15.5 mm<sup>2</sup>; measuring accuracy  $\pm 0.04$   $\mu\text{m}$ ; dashed lines only to guide the eye)

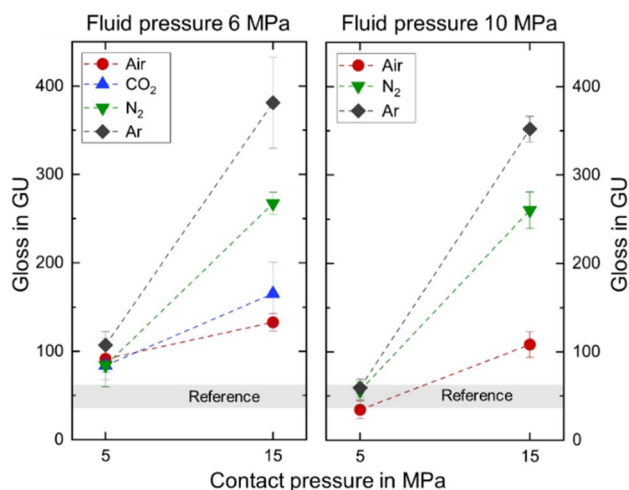


**Fig. 11** Results of the gloss measurements of the worn strips in dependence of the different lubrication media, contact—and fluid pressure (reference measured before drawing process; measuring area 72 mm<sup>2</sup>; error bars  $\pm$  sample standard deviation; dashed lines only to guide the eye)

temperature the friction behavior is comparable to those of bare zinc [33, 34], especially in case of a roughly closed zinc oxide surface layer [35]. Here, adhesion effects and the regeneration of the ZnO surface layer can cause partial wear debris, which can lead to an increasing abrasive wear and the observed scratches.

Variance analysis (ANOVA) for the gloss measurements of Fig. 11 showed no significant differences for the investigations at  $p_N = 5$  MPa. However, significant, e.g. highly significant, differences at  $p_N = 15$  MPa (except air-CO<sub>2</sub> at  $p_F =$

6 MPa;  $p$ -values  $\leq 0.001$ ) were measured. With a decrease of 0.54  $\mu\text{m}$  in surface roughness and an increase of 109 GU compared to the reference at a contact pressure of 15 MPa, lubricating with CO<sub>2</sub> led to very low wear. From cryogenic machining with liquid N<sub>2</sub> it is known that decreasing temperatures in the contact area changes yielding stress, shear strength and local material hardness which can lead to a reduction of the friction coefficient [36, 37]. As shown in Sect. 3.1, the local surface temperatures, when using liquid CO<sub>2</sub>, can decrease below 220 K. In comparison to the temperatures reached in cryogenic machining these are even high temperatures. However, as shown by Gård et al. [38], the adhesive wear and in relation also the friction coefficient is mainly influenced by the material temperature. A decreasing temperature leads to less adhesive wear, which is especially important while drawing aluminum and zinc-coated sheets [39, 40]. Thus, the drop in temperature of the surface when using liquid CO<sub>2</sub> can also be found as a reason for the measured low wear and low friction coefficients. Besides this effect, as discussed, the higher fluid pressure in the contact zone and the dry ice formation (cf. Sect. 3.1) can cause such low wear.

In contrast, the highest measured wear, especially at high contact pressures, was obtained by using Ar as volatile lubricant. As the passivation layer of zinc was ruttled during the drawing process, the tool surface got in contact with the bare zinc. The Ar atmosphere acts as a protective gas, preventing the formation of oxides and carbonates (cf. Sect. 3.3). Thus, the chemical tribology is comparable to those in vacuum atmosphere. Several studies examined the tribology of dry sliding metal contacts in vacuum [41, 42], showing a higher tendency to adhesive wear and consequently high friction coefficients. However, as mentioned, the adhesions on the tools by using Ar seemed relatively low. This leads to the assumption, that adhesion effects on the tool surface occurred relatively fast in limited areas. Since these adhesions were visible on the tool surfaces subsequent to the process a stronger bonding of the adhesions to the tool than the metallic bonding in the zinc is supposed. Thus, only low adhesions are sufficient to create strong abrasive wear and to smooth the whole sheets surface, especially at high contact pressures.

The wear when using N<sub>2</sub> as lubricant was consequently high, but lower than those of Ar. Fundamentally comparable effects to Ar lubrication occurred. One difference is the ability of N<sub>2</sub> to adsorb on metal surfaces, which leads to a very thin surface layer and reduces the adhesive wear [10, 43, 44]. In addition, the slightly higher pressure in the contact zone compared to Ar decreases the wear, as shown in Fig. 11. Overall it can be noted, that the measured gloss values of the worn surfaces correlate and confirm the surface roughness measurements. Thus, this investigation can be seen as a

quick evaluation method of the wear of zinc-coated surfaces, also for production processes.

### 3.3 Changes in Chemical Surface Composition During Drawing

The chemical analysis was made to investigate any chemical changes of the surface caused by the drawing process or the used lubrication media (air, CO<sub>2</sub>, N<sub>2</sub>, Ar). As the measurements were performed on the zinc-coated strips after the strip drawing experiments, the mainly detected elements were C, O and Zn (cf. Fig. 12). In addition, small amounts of Ca could be found. The corrosion protection of zinc is based on the formation of ZnO and ZnCO<sub>3</sub> or in humid environment rather different zinc hydroxycarbonates [45]. As the binding energies of the carbonates are similar and the samples contain a variety of different other chemical compounds, an exact allocation of the measured elements to the types of carbonates is not possible within this study.

The Zn 2p spectrum contains two spin-orbit peaks at 1046 eV (1/2) and 1022.3 eV (3/2). For the investigation

only the 3/2-peak was evaluated and split into two sub peaks at 1022.6 eV and 1023.6 eV, relating to bare zinc / zinc oxide and zinc carbonates, respectively [46]. The O 1s spectrum can be fitted by three curves with maxima at 530.9 eV allocated to oxides (mainly ZnO), 532 eV assigned to organic contaminants and 533.3 eV assigned to carbonates [47, 48]. The C 1s spectrum is also split into three peaks: the first at 284.9 eV allocated to aliphatic hydrocarbon contaminations, the second at 286.4 eV assigned to C–O compounds from residue oil additives and other contaminants and the third at 290.6 eV allocated to inorganic carbon (mostly carbonates).

In Table 2, the surface composition as a result of the XPS measurements and the aforementioned allocation is shown in atom percentage. The small amounts of Ca can be explained by the acetone precleaning of the metal strips as a residue of the acetone production from calcium acetate. The high organic carbon content of the reference is caused by residues of the protection oil of the sheet metal as well as deposits from the environment. After the drawing process, the organic carbon was reduced for all lubricants because of wear and shear forces at the surface initiated by the high flow

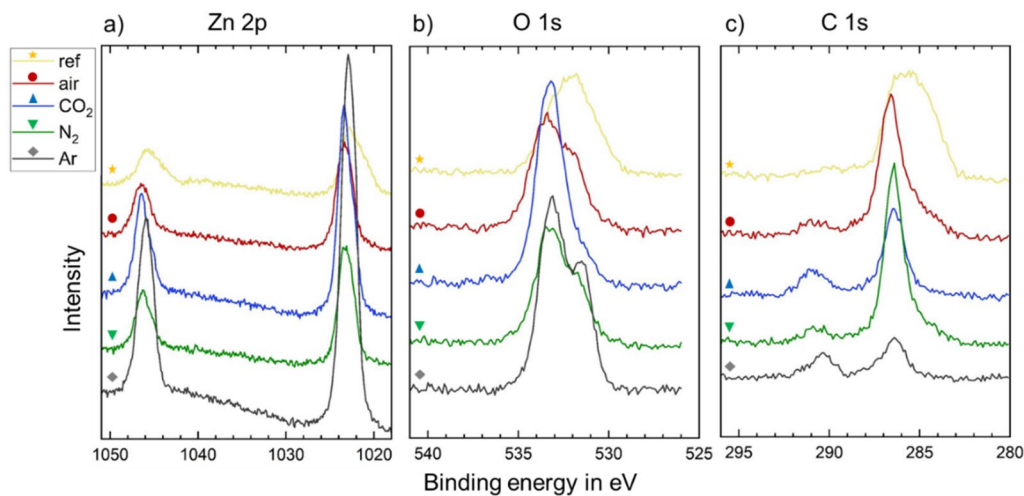


**Fig. 12** Selected electron energy spectra for zinc (a), oxygen (b) and carbon (c), measured by XPS of the zinc-coated sheet metal; reference (ref) before drawing and drawn with different volatile lubricants

**Table 2** Quantification overview of the chemical analysis results of the reference and the worn strips drawn with different lubrication fluids (in atom percentage)

Element Lubricant	C organic hydro- carbon	C organic others	C inorganic	O oxides	O organic	O carbonates	Ca oxides/car- bonates	Zn bare/oxide	Zn carbonates
Ref.	31.9	27.2	2.5	10	11.6	6.2	0.8	9.8	–
Air	8.7	39.4	7.5	7.2	2.8	19.8	1.6	12.9	–
CO <sub>2</sub>	1.9	23.6	11.4	4.3	0.4	36	0.7	18.9	2.9
N <sub>2</sub>	5.9	42.6	7.1	6.4	5.1	18.3	1.1	13	0.4
Ar	0.5	10.4	8.5	13.3	2.4	28.5	–	36.3	–

velocities of the lubricants. By using Ar, the effect of wear on the surface chemistry can be recognized distinctively. In contrast, the reduction of the organic carbon content on the surface by using CO<sub>2</sub> as lubricant is mainly caused by a cleaning effect of the medium. Dry-ice blasting is a well-known technique for cleaning surfaces even for removing volatile organic compounds (VOCs) [49, 50]. Although CO<sub>2</sub> is relatively inert and has no electric dipole moment, the Van der Waals interaction energy of the liquid phase with other particles is very high [51]. As mentioned, the CO<sub>2</sub> is usually passed to solid and gaseous state before hitting the sheet metal surface. Nevertheless, partially liquefaction can occur, caused by the dynamic pressure in the center of the jet. In addition, an adsorption of the contaminants on the surface of the dry ice can contribute to the cleaning effect.

The increase of inorganic carbon in relation to the reference for all lubricants is driven by the percentage decrease of the organic carbon. However, in comparison to other media, when using CO<sub>2</sub> a greater increase was measured. This can be explained by the formation of zinc carbonates as, in the presence of CO<sub>2</sub>, ZnO converts to ZnCO<sub>3</sub>. Consequently, this process is well-advanced as the sheets are usually aged in ambient air. Thus, the reference is supposed to contain carbonates as well. As mentioned, the exact allocation of the zinc carbonates is not possible and additionally, in case of the reference, contaminants obscure the measurement of ZnCO<sub>3</sub>. Therefore, the real amount of zinc carbonates was expected probably higher for all samples. However, taking the measured amounts of inorganic carbon and oxygen from carbonates into account, a significant increase of carbonates by using CO<sub>2</sub> is obvious. To prevent white rust, the formation of ZnCO<sub>3</sub> is a desired process. Thus, the drawing process with liquid CO<sub>2</sub> is not just only dry, but can help to prepare the parts for further process steps such as coating or joining by cleaning and passivating the surface. The sharp increase of ZnO by using Ar is caused by wear as a very thin surface zinc oxide layer forms from bare zinc in the time of handling in ambient air before and after packaging airtight. In all measurements, no iron could be found, so, despite of wear effects, the zinc coating was still closed and the wear of the tools was not measurable. The presented findings are related to the use of electrogalvanized sheet metal, however investigations [52] showed similar behavior when using hot-dip galvanized steel sheets. Even with uncoated DC05 sheet metal, promising findings regarding friction and wear were made.

By using air or N<sub>2</sub> as lubricants, the measured chemical composition of the surface after the drawing process was almost similar. Thus, the lubrication by air seems to have no promoting influence on the amount of ZnO on the surface. However, the measurements could not finally clarify the influence of the oxygen entailed in the lubricant air. This is due to the following three conditions: First, a clear

distinction between bare Zn and ZnO is difficult, second, the ZnO formation takes place right after the drawing process and third, the surfaces of the metal strips drawn under air are inhomogeneous. Nevertheless, during the drawing process under air lubrication a higher ZnO concentration is likely resulting in higher wear. The O<sub>2</sub> content of the lubricant can also cause the increasing friction and wear values by raising air pressure at high contact pressures (cf. Figs. 8 and 10).

## 4 Conclusion

Volatile media, especially CO<sub>2</sub>, are suitable for dry deep drawing processes and specific recommendations for the use of this new tribological system can now be given. The presented findings are related to the use of zinc coated sheet metal, however a similar behavior is suggested when using uncoated steel sheets. Starting from numerous basic investigations up to drawing tests, the research presented here focused on tribological and tribochemical investigations of the suitability of different fluids (air, liquid CO<sub>2</sub>, N<sub>2</sub> and Ar) as volatile lubricants. New strip drawing jaws were designed or rather optimized with regard to minimal elastic deformation and manufactured for these investigations. Thus, the influence of the elastic deformation on the tribological behavior could be evaluated as insignificant. For producing the at least 5 mm deep and defined conical shaped micro holes, a depth-adapted laser drilling strategy was developed in which the focus of the laser beam moves along a spiral path and the focal plane was shifted incrementally (adjusted to the drilling process) below the surface of the drawing jaw.

Fluid dynamics simulations were performed, especially for CO<sub>2</sub>, showing a high acceleration of the fluid in the micro hole and the contact zone which leads to dry ice formation. Temperatures in CO<sub>2</sub> dropped to approx. 200 K, cooling the surface partially to temperatures below 220 K. In contrast to lubrication with CO<sub>2</sub>, the other media studied (air, N<sub>2</sub>, Ar) showed only a minor cooling effect. Besides the cooling, CO<sub>2</sub> triggers a higher pressure in the contact zone and consequently lower friction and wear, since it passes the narrowest part still in the liquid state. Thus, the formation of dry ice, the cooling of roughness peaks, the higher pressure in the contact zone and the formation of zinc carbonate as a solid lubricant caused the lowest measured friction and wear when using CO<sub>2</sub> of all investigated lubricants. Furthermore, the chemical analyses showed a cleaning and passivating effect of the CO<sub>2</sub> drawn strips. To summarize, liquid CO<sub>2</sub> showed the most promising results for dry deep drawing process lubrication.

In contrast, the highest friction and wear were found when Ar was used. The XPS measurement performed on the sheet sample drawn with Ar showed a reorganization of the surface as the former interface was completely worn.

The use of air showed medium friction coefficients but local heavy wear due to oxidation processes in the contact area and subsequently partial single deep scratches in the zinc surface. Thus, Ar and air appeared to be unfavorable for the lubrication of drawing processes. With N<sub>2</sub> as lubricant, moderate friction and wear were measured. Therefore, for processes with only low contact forces or when moderate friction and wear are acceptable, N<sub>2</sub> lubrication may be a relatively low-cost and environment friendly option.

By using the volatile lubricants presented here, it is possible to achieve the aforementioned goals of improved sustainability, environmental protection and pollutant reduction in the production of deep drawn sheet metal components. This is mainly due to the substitution of conventional oil-based lubricants including additives that are harmful to health and environment and the shortening of the process chain around oil application, component cleaning and disposal of the cleaning residues. In addition, it is based on a significant improvement in process stability, especially in the connection with CO<sub>2</sub>. This new tribological system thus contributes to achieving environmental and climate goals and can provide an economic benefit by saving investment costs for oil application and component cleaning.

**Acknowledgements** The authors would like to thank J. H. Henze from Fraunhofer IGB for his support and the profound discussions. His assistance was especially helpful in regard to the chemical analysis.

**Funding** Open Access funding enabled and organized by Projekt DEAL. The scientific investigations of this paper were funded by the German Research Foundation (DFG) within the priority program SPP 1676 Dry Metal Forming—Sustainable Production by Dry Processing in Metal Forming. We thank the DFG for the funding of this research project.

## Declarations

**Conflict of interest** The authors declare that there is no financial interest, personal relationship or other conflict of interest that could have influenced this work.

**Open Access** This article is licensed under a Creative Commons Attribution 4.0 International License, which permits use, sharing, adaptation, distribution and reproduction in any medium or format, as long as you give appropriate credit to the original author(s) and the source, provide a link to the Creative Commons licence, and indicate if changes were made. The images or other third party material in this article are included in the article's Creative Commons licence, unless indicated otherwise in a credit line to the material. If material is not included in the article's Creative Commons licence and your intended use is not permitted by statutory regulation or exceeds the permitted use, you will need to obtain permission directly from the copyright holder. To view a copy of this licence, visit <http://creativecommons.org/licenses/by/4.0/>.

## References

- Vollertsen, F., & Schmidt, F. (2014). Dry metal forming: definition, chances and challenges. *International Journal of Precision Engineering and Manufacturing-Green Technology*, 1(1), 59–62. <https://doi.org/10.1007/s40684-014-0009-0>.
- Bay, N., Azushima, A., Groche, P., Ishibashi, I., Merklein, M., Morishita, M., Nakamura, T., Schmid, S., & Yoshida, M. (2010). Environmentally benign tribo-systems for metal forming. *CIRP Annals*, 59(2), 760–780. <https://doi.org/10.1016/j.cirp.2010.05.007>.
- Böhmermann, F., Herrmann, M., Riemer, O., & Kuhfuss, B. (2018). Reducing abrasive particle generation in dry rotary swaging by utilizing DLC hard coated dies. *MATEC Web of Conferences*, 190, 14011. <https://doi.org/10.1051/mateconf/201819014011>
- Zhao, R., Steiner, J., Andreas, K., Merklein, M., & Tremmel, S. (2018). Investigation of tribological behaviour of a-C:H coatings for dry deep drawing of aluminium alloys. *Tribology International*, 118, 484–490. <https://doi.org/10.1016/j.triboint.2017.05.031>.
- Zahedi, E., Woerz, C., Reichardt, G., Umlauf, G., Liewald, M., Barz, J., Weber, R., Foerster, D. J., & Graf, T. (2019). Lubricant-free deep drawing using CO<sub>2</sub> and N<sub>2</sub> as volatile media injected through laser-drilled microholes. *Manufacturing Review*, 6, 11. <https://doi.org/10.1051/mfreview/2019011>
- Reichardt, G., Henn, M., Reichle, P., Umlauf, G., Riedmüller, K., Weber, R., Barz, J., Liewald, M., Graf, T., & Tovar, G. E. M. (2021). Friction and wear behavior of deep drawing tools using volatile lubricants injected through laser-drilled micro-holes. *Jom Journal Of The Minerals Metals And Materials Society*. <https://doi.org/10.1007/s11837-021-05028-8>.
- Peng, S., Li, T., Tang, Z., Shi, J., & Zhang, H. (2016). Comparative life cycle assessment of remanufacturing cleaning technologies. *Journal of Cleaner Production*, 137, 475–489. <https://doi.org/10.1016/j.jclepro.2016.07.120>.
- Pereira, O., Rodríguez, A., Fernández-Abia, A. I., Barreiro, J., & López de Lacalle, L. N. (2016). Cryogenic and minimum quantity lubrication for an eco-efficiency turning of AISI 304. *Journal of Cleaner Production*, 139, 440–449. <https://doi.org/10.1016/j.jclepro.2016.08.030>.
- Liewald, M., Würz, C., & Riedmüller, K. R. (2021). Characterization of a novel aerostatic lubrication system for deep drawing processes. *CIRP Annals*, 70(1), 239–242. <https://doi.org/10.1016/j.cirp.2021.03.013>.
- Bowden, F. P. (1939). The friction of clean metals and the influence of adsorbed gases. The temperature coefficient of friction. *Proceedings of the Royal Society of London. Series A, Mathematical and Physical Sciences*, 172(949), 263–279.
- Mishina, H. (1992). Atmospheric characteristics in friction and wear of metals. *Wear*, 152(1), 99–110. [https://doi.org/10.1016/0043-1648\(92\)90207-O](https://doi.org/10.1016/0043-1648(92)90207-O).
- Velkavrh, I., Ausserer, F., Klien, S., Brenner, J., Forêt, P., & Diem, A. (2014). The effect of gaseous atmospheres on friction and wear of steel–steel contacts. *Tribology International*, 79, 99–110. <https://doi.org/10.1016/j.triboint.2014.05.027>.
- Zhang, Y., & Jourani, A. (2021). Combined effect of microstructure and gaseous environments on oxidative and Adhesive wear of dual-phase steel. *Journal of Materials Engineering and Performance*. <https://doi.org/10.1007/s11665-021-06090-8>.
- Cai, Z., Zhu, M., Zheng, J., Jin, X., & Zhou, Z. (2009). Torsional fretting behaviors of LZ50 steel in air and nitrogen. *Tribology International*, 42, 11–12. <https://doi.org/10.1016/j.triboint.2009.04.031>.

15. de Mello, J. D. B., & Binder, R. (2012). Tribocamada formada em revestimentos multifuncionais: Influência do ambiente. *Tecnologia em Metalurgia Materiais e Mineração*, 9(2), 81–88. <https://doi.org/10.4322/tmm.2012.013>
16. Wu, X., Cong, P., Nanao, H., Minami, I., & Mori, S. (2004). Tribological behaviors of 52100 steel in Carbon Dioxide Atmosphere. *Tribology Letters*, 17(4), 925–930. <https://doi.org/10.1007/s11249-004-8101-1>
17. Wörz, C., Liewald, M., & Singer, M. (2016). Investigation of tribological conditions in the strip drawing test using liquid CO<sub>2</sub> and N<sub>2</sub> as a volatile lubricant. In *7th International conference on tribology in manufacturing processes* (pp. 140–148). ISBN: 978-616-92565-0-2.
18. Singer, M., & Liewald, M. (2015). Evaluation of different influencing factors in dry sheet metal forming with vaporizing CO<sub>2</sub> used as lubricant. *Applied Mechanics and Materials*, 794, 53–58. <https://doi.org/10.4028/www.scientific.net/AMM.794.53>
19. Henn, M., Reichardt, G., Weber, R., Graf, T., & Liewald, M. (2020). Dry metal forming using volatile lubricants injected into the forming tool through flow-optimized, laser-drilled microholes. *JOM*, 72(7), 2517–2524. <https://doi.org/10.1007/s11837-020-04169-6>
20. Reichardt, G., & Liewald, M. (2022). Characterization of an environmentally friendly Tribological System for Deep drawing using volatile media as Lubricant Substitute. *Defect and Diffusion Forum*, 414, 75–80. <https://doi.org/10.4028/p-65utsh>
21. Weber, R., Graf, T., Berger, P., Onuseit, V., Wiedenmann, M., Freitag, C., & Feuer, A. (2014). Heat accumulation during pulsed laser materials processing. *Optics Express*, 22(9), 11312–11324. <https://doi.org/10.1364/OE.22.011312>
22. Förster, D. J., Weber, R., Holder, D., & Graf, T. (2018). Estimation of the depth limit for percussion drilling with picosecond laser pulses. *Optics Express*, 26(9), 11546–11552. <https://doi.org/10.1364/OE.26.011546>
23. Holder, D., Weber, R., Graf, T., Onuseit, V., Brinkmeier, D., Förster, D. J., & Feuer, A. (2021). Analytical model for the depth progress of percussion drilling with ultrashort laser pulses. *Applied Physics A*, 127, 5. <https://doi.org/10.1007/s00339-021-04455-3>
24. Negel, J. P., Voss, A., Abdou Ahmed, M., Bauer, D., Sutter, D., Killi, A., & Graf, T. (2013). 1.1 kW average output power from a thin-disk multipass amplifier for ultrashort laser pulses. *Optics Letters*, 38(24), 5442–5445. <https://doi.org/10.1364/OL.38.005442>
25. Liewald, M., Tovar, G. E. M., Woerz, C., & Umlauf, G. (2020). Tribological conditions using CO<sub>2</sub> as volatile lubricant in Dry Metal Forming. *International Journal of Precision Engineering and Manufacturing-Green Technology*, 7(5), 965–973. <https://doi.org/10.1007/s40684-019-00069-6>
26. Bhattacharyya, S. (Ed.) (2022). *Applications of computational fluid dynamics simulation and modeling: Turbulence models commonly used in CFD*. London: IntechOpen. <https://doi.org/10.5772/intechopen.94665>
27. Peng, D. Y., & Robinson, D. B. (1976). A new two-constant equation of state. *Industrial and Engineering Chemistry Fundamentals*, 15(1), 59–64. <https://doi.org/10.1021/i160057a011>
28. American Galvanizers Association. (2022). Corrosion protection for steel. Retrieved from <http://galvanizeit.org/hot-dip-galvanizing/why-specify-galvanizing/corrosion-protection>. Accessed 21 Dec 2022
29. Zhang, X. G. (Ed.). (1996). *Corrosion and electrochemistry of zinc*. Springer. <https://doi.org/10.1007/978-1-4757-9877-7>
30. Hamrock, B. J., Schmid, S. R., & Jacobson, B. O. (Eds.). (2004). *Fundamentals of fluid film lubrication*. Dekker.
31. Wörz, C., Reichardt, G., Liewald, M., Zahedi, E., Weber, R., & Graf, T. (2018). Dry deep drawing of a rectangular cup assisted by volatile media injected from laser-drilled microholes. *Dry Metal Forming OAJ FMT*, 4, 1–8.
32. Reichardt, G., Henn, M., Reichle, P., Hemming, D., Umlauf, G., Riedmüller, K., Weber, R., Barz, J., Liewald, M., Graf, T., & Tovar, G. E. M. (2021). *Investigations on the process stability of dry deep drawing with volatile lubricants injected through laser-drilled microholes* (pp. 230–246). [https://doi.org/10.1007/978-3-030-65261-6\\_21](https://doi.org/10.1007/978-3-030-65261-6_21)
33. Yang, J. F., Jiang, Y., Hardell, J., Prakash, B., & Fang, Q. F. (2013). Influence of service temperature on tribological characteristics of self-lubricant coatings: a review. *Frontiers of Materials Science*, 7(1), 28–39. <https://doi.org/10.1007/s11706-013-0190-z>
34. Wilson, R. (1952). Part I. Friction of metals—Influence of oxide films on metallic friction. *Proceedings of the Royal Society of London, Series A, Mathematical and Physical Sciences*, 212(1111), 450–452. <https://doi.org/10.1098/rspa.1952.0247>
35. Zabinski, J. S., Corneille, J., Prasad, S. V., Mc Devitt, N. T., & Bultman, J. B. (1997). Lubricious zinc oxide films: Synthesis, characterization and tribological behaviour. *Journal of Materials Science*, 32(20), 5313–5319. <https://doi.org/10.1023/A:1018614811131>
36. Hong, S. Y., Ding, Y., & Jeong, J. (2002). Experimental evaluation of friction coefficient and liquid nitrogen lubrication effect in cryogenic machining. *Machining Science and Technology*, 6(2), 235–250. <https://doi.org/10.1081/MST-120005958>
37. Hong, S. Y. (2006). Lubrication mechanisms of LN<sub>2</sub> in ecological cryogenic machining. *Machining Science and Technology*, 10(1), 133–155. <https://doi.org/10.1080/10910340500534324>
38. Gåård, A., Hallbäck, N., Krakhmalev, P., & Bergström, J. (2010). Temperature effects on adhesive wear in dry sliding contacts. *Wear*, 268, 7–8. <https://doi.org/10.1016/j.wear.2009.12.007>
39. Groche, P., & Nitzsche, G. (2007). Influence of temperature on the initiation of adhesive wear with respect to deep drawing of aluminum-alloys. *Journal of Materials Processing Technology*, 191(1–3), 314–316. <https://doi.org/10.1016/j.jmatprotec.2007.03.098>
40. Deuis, R. L., Subramanian, C., & Yellup, J. M. (1997). Dry sliding wear of aluminium composites—A review. *Composites Science and Technology*, 57(4), 415–435. [https://doi.org/10.1016/S0266-3538\(96\)00167-4](https://doi.org/10.1016/S0266-3538(96)00167-4)
41. Buckley, D. H. (1971). *Friction, wear, and lubrication in vacuum*. National Aeronautics and Space Administration.
42. Miyoshi, K. (1999). Considerations in vacuum tribology (adhesion, friction, wear, and solid lubrication in vacuum). *Tribology International*, 32(11), 605–616. [https://doi.org/10.1016/S0301-679X\(99\)00093-6](https://doi.org/10.1016/S0301-679X(99)00093-6)
43. Mishina, H. (1995). Chemisorption of diatomic gas molecules and atmospheric characteristics in adhesive wear and friction of metals. *Wear*, 180(1–2), 1–7. [https://doi.org/10.1016/0043-1648\(95\)80003-4](https://doi.org/10.1016/0043-1648(95)80003-4)
44. Velkavrh, I., Ausserer, F., Klien, S., Voyer, J., Ristow, A., Brenner, J., Forêt, P., & Diem, A. (2016). The influence of temperature on friction and wear of unlubricated steel/steel contacts in different gaseous atmospheres. *Tribology International*, 98, 155–171. <https://doi.org/10.1016/j.triboint.2016.02.022>
45. Kasperrek, J., Verchere, D., Jacquet, D., & Phillips, N. (1998). Analysis of the corrosion products on galvanized steels by FTIR spectroscopy. *Materials Chemistry and Physics*, 56(3), 205–213. [https://doi.org/10.1016/S0254-0584\(98\)00167-9](https://doi.org/10.1016/S0254-0584(98)00167-9)
46. Wagner, C. D. (1975). Chemical shifts of Auger lines, and the Auger parameter. *Faraday Discussions of the Chemical Society*, 60, 291. <https://doi.org/10.1039/dc9756000291>
47. Liu, Z., & Teng, F. (2018). Understanding the correlation of crystal atoms with photochemistry property: Zn<sub>5</sub>(OH)<sub>6</sub>(CO<sub>3</sub>)<sub>2</sub> vs ZnCO<sub>3</sub>. *Chemistry Select*, 3(31), 8886–8894. <https://doi.org/10.1002/slct.201801420>
48. Verma, D. K., Kumar, B., & Kavita, Rastogi, R. B. (2019). Zinc oxide- and magnesium-doped zinc oxide-decorated

nanocomposites of reduced graphene oxide as friction and wear modifiers. *ACS Applied Materials and Interfaces*, 11(2), 2418–2430. <https://doi.org/10.1021/acsami.8b20103>

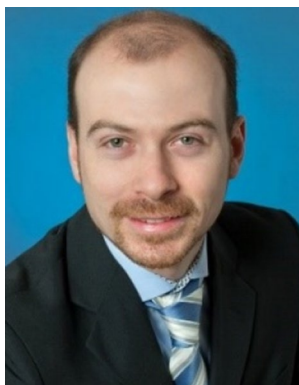
49. Spur, G., Uhlmann, E., & Elbing, F. (1999). Dry-ice blasting for cleaning: Process, optimization and application. *Wear*, 233–235, 402–411. [https://doi.org/10.1016/S0043-1648\(99\)00204-5](https://doi.org/10.1016/S0043-1648(99)00204-5)
50. Keller, M., Ernst, C., & Grimme, R. (2011). Reinigung und reinheitskontrolle von medizinprodukten (article in German). *Medi-ironic-Journal Nr*, 2, 14–16.
51. Banerjee, S., Sutanto, S., Kleijn, J. M., van Roosmalen, M. J. E., Witkamp, G. J., & Stuart, M. A. C. (2012). Colloidal interactions in liquid Co<sub>2</sub>—A dry-cleaning perspective. *Advances in Colloid and Interface Science*, 175, 11–24. <https://doi.org/10.1016/j.cis.2012.03.005>
52. Wörz, C. (2020). *Aufbau und Charakterisierung von aero-statischen Schmiersystemen für das Tiefziehen* (article in German). Institut für Umformtechnik. <https://doi.org/10.18419/opus-11169>

**Publisher's Note** Springer Nature remains neutral with regard to jurisdictional claims in published maps and institutional affiliations.



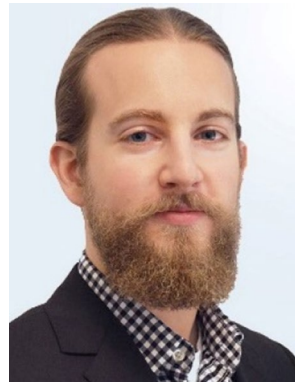
**Paul Reichle** is a research engineer in the department of Chemical and Physical Interfaces and a doctoral candidate at the Institute of Interfacial Process Engineering and Plasma Technology (IGVP) at the University of Stuttgart. He studied sustainable engineering and mechanical engineering at the Universities of Applied Sciences Esslingen and Konstanz, respectively. In close cooperation with the department of Functional Surfaces and Materials from the Fraunhofer Institute IGB he is researching in

the fields of surface modification and plasma coating for reducing friction, wear and to adjust wetting properties.

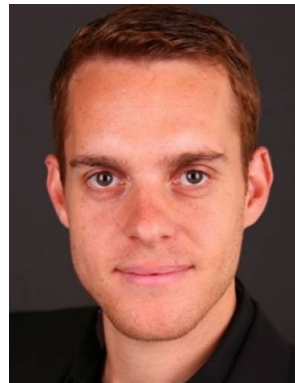


**Gerd Reichardt** is a research engineer in the department of Sheet Metal Forming and Cutting Processes at the Institute for Metal Forming Technology (IFU) at the University of Stuttgart. After his Master's at the Nuremberg Institute of Technology and Bachelor's at the University of Applied Sciences Ulm in mechanical engineering he is researching in the field of tribology and wear of sheet metal forming processes. Especially sustainable and environmentally friendly tribological systems are

the main focus of his research activity.



**Manuel Henn** received his master's degree in mechanical engineering from the University of Erlangen-Nürnberg. In 2019, he joined the Institut für Strahlwerkzeuge IFSW at the University of Stuttgart as a scientific employee. There he is part of the research group for laser process development and precision machining and works on projects such as microdrilling with ultrashort pulse lasers and the combination of additive and subtractive laser-based processes as part of the Innovation Campus Mobility of the Future.



**Georg Umlauf** has been at Fraunhofer IGB since 2013. Umlauf studied mechatronics, specializing in "special manufacturing methods", at the TU Dresden. In 2020, he completed his PhD in process engineering with studies on the application of carbon dioxide as a volatile lubricant in dry metal forming at the Institute of Interfacial Process Engineering and Plasma Technology (IGVP) at the University of Stuttgart. Since 2018, he has been working as a researcher in the innovation field of Func-

tional Surfaces and Materials in the department of plasma processes at the Fraunhofer Institute IGB in Stuttgart.



**Jakob Barz** is Senior Scientist at the Fraunhofer Institute for Interfacial Engineering and Biotechnology IGB, Stuttgart, and principal investigator at the Institute for Interfacial Engineering and Plasma Technology IGVP at Stuttgart University. He joined Fraunhofer in 2003 after finishing his Diploma in Physics at Stuttgart University. In 2010, he received his PhD on a plasma-chemical topic at the former Institute for Plasma Research, IPF, Stuttgart. His focusses of research are plasma processes as

well as surface and interface analysis.



**Kim Rouven Riedmüller** is a research engineer at the Institute for Metal Forming Technology (IFU) at the University of Stuttgart. In 2018, he completed his doctoral thesis in mechanical engineering with the topic “Design of a process route for thixoforging of metallic semi-finished tubes taking into account occurring material flows”. Since 2013, he is the head of the department “Semi-solid Forming” at IFU, where he has additionally assumed the leadership of the department

“Sheet Metal Forming and Cutting Processes” in 2018.



**Mathias Liewald** is the head of the Institute for Metal Forming Technology (IFU) at the University of Stuttgart. After his doctoral thesis in the research field of sheet metal forming in 1990 at the University of Dortmund, he worked in various management positions at well-known companies in the automotive industry from 1991 to 2005. In 2005, he became the director of the Institute for Metal Forming Technology at the University of Stuttgart. Since the beginning of this activity, he has dedicated himself

to scientific research in the areas of extending process limits, modelling the elastoplastic behaviour of metallic materials and increasing the

manufacturing stability of sheet metal forming, cold forging and semi-solid forming processes. He is also involved in numerous scientific organisations and acts as a peer reviewer.



**Günter E. M. Tovar** directs the Institute of Interfacial Process Engineering and Plasma Technology (IGVP) at the University of Stuttgart since 2015. Previously, he studied chemistry with a focus on physical chemistry and chemical technology at the Technical University of Darmstadt, Germany, the Université de Bordeaux and at the CNRS CEMES in Toulouse, both France. He conducted his doctorate at the Max Planck Institute for Polymer Research and the Johannes-Gutenberg-University

in Mainz, Germany, and at RIKEN, the Institute of Physical and Chemical Research, Wako near Tokyo, Japan, and habilitated at the University of Stuttgart. His research interests include nanomaterials technology, medical technology, and environmental engineering, and he draws inspiration from the United Nations Sustainable Development Goals.